Renewable Energy 173 (2021) 768–780

Contents lists available at ScienceDirect

Renewable Energy

journal homepage: www.elsevier.com/locate/renene

Thermal performance analysis of packed-bed thermal energy storage with radial gradient arrangement for phase change materials

Wei Wang [a, b], Xibo He [a, b], Yicheng Hou [a, b], Jun Qiu [a, b], Dongmei Han [a, b], Yong Shuai [a, b, *]

[a] School of Energy Science and Engineering, Harbin Institute of Technology, Harbin, 150001, China
[b] Key Laboratory of Aerospace Thermophysics, Ministry of Industry and Information Technology, Harbin, 150001, China

ARTICLE INFO

Article history:
Received 31 October 2020
Received in revised form
22 February 2021
Accepted 5 April 2021
Available online 12 April 2021

Keywords:
Thermal energy storage
Packed-bed
Phase change materials
Thermal performance analysis
Radial gradient arrangement

ABSTRACT

The current paper investigates the radial gradient arrangement of phase change material capsules effect on the thermal behavior of a packed-bed latent thermal energy storage system. A transient two-dimensional dispersion-concentric model is developed to analyze the phase transition of phase change materials. Moreover, the heat transfer characteristics between air and phase change material capsules in four different packed bed systems are discussed in detailed. The results indicate that the use of radial gradient arrangement in the phase change material capsules significantly enhances the heat transfer performance of the system. The system pressure drop is apparently decreased when the radial gradient arrangement is taken into consideration. From case 1 to case 4, the overall energy efficiency is 84.16%, 80.43%, 83.55%, and 82.46%, respectively. The capacity ratio of case 1 is higher than all studied cases by 5.03%, 1.11%, and 3.74%, respectively. The utilization ratio of case 1 is higher than all studied cases by 5.15%, 1.45%, and 3.43%, respectively. Furthermore, considering the loss of pressure drop, it is found that case 3 is the most viable option of all the studied cases. This study provides a numerical basis for the thermal stability output and the structure optimization of packed bed system.

1. Introduction

Solar energy has been widely used through solar thermal utilization [1,2], solar photovoltaic [3,4], solar fuels technologies [5,6], and some emerging technologies [7,8]. Because of the unstable and intermittent nature of solar energy resources, the integration of thermal energy storage (TES) system in the concentrating solar power (CSP) systems play an important role to improve the stability of the power generation system and the energy utilization efficiency [9–11]. TES systems can be classified into three main categories of sensible heat, latent heat, and thermochemical heat [12,13]. The latent thermal energy storage (LTES) system using phase change materials (PCM) has attracted lots of attention in recent years due to the advantages of high energy density, quasi-isothermal charging/discharging processes, and reasonable capital investment [14–16]. The schematic layout of a CSP hybrid power plant using the packed-bed LTES with spherical PCM capsules, as illustrated in Fig. 1. The hot air could be stored in a packed-bed LTES for further applications, such as through the heat exchanger to heat a secondary working fluid for the power cycle. During the gas turbine power generation process, the hot gas discharged from the turbine will pass through a heat recovery/heat exchanger, which uses waste heat to preheat water by the steam turbine power generation. The cooling air is further cooled for stage compression, which improves compressor efficiency [17].

1.1. The packed bed LTES system

Among the high-temperature LTES systems, the packed bed system is considered one of the most popular configurations for commercial and industrial applications [18]. Compared with the commonly used two-tank heat storage, the single-tank packed bed LTES has higher heat storage density and smaller volume, and the heat storage cost can reduce by 20%–37% [19]. Many scholars focused on the numerical study on the thermal behavior of the TES thermocline tank because of the complex dynamic nature of this system, and the laboratory experiments are also difficult to conduct. Therefore, it was imperative to review the various numerical methods that were used to study and simulate the process

* Corresponding author. School of Energy Science and Engineering, Harbin Institute of Technology, Harbin, 150001, China.
E-mail addresses: solarwangwei@163.com (W. Wang), qiujun@hit.edu.cn (J. Qiu), shuaiyong@hit.edu.cn (Y. Shuai).

https://doi.org/10.1016/j.renene.2021.04.032
0960-1481/

Nomenclatures

C_F	inertial coefficient
c_p	specific heat capacity, $J \cdot kg^{-1}\ K^{-1}$
D	tank diameter, m
d_p	spherical capsule diameter, m
g	acceleration due to gravity, $m \cdot s^{-2}$
H	tank height, m
h	heat transfer coefficient, $W \cdot m^{-2}\ K^{-1}$
h_i	inner heat transfer coefficient, $W \cdot m^{-2}\ K^{-1}$
h_s	heat transfer coefficient at the capsule surface, $W \cdot m^{-2}\ K^{-1}$
h_v	volumetric interstitial heat transfer coefficient, $W \cdot m^{-3}\ K^{-1}$
h_w	overall heat transfer coefficient, $W \cdot m^{-2}\ K^{-1}$
K	intrinsic permeability of porous medium, m^2
k	thermal conductivity, $W \cdot m^{-1}\ K^{-1}$
L	latent heat, J/kg
Nu	Nusselt number
ΔP	pressure drop, Pa
p	pressure, Pa
Pr	Prandtl number
Ra	Rayleigh number
Re	Reynolds number
r	radius, m
T	temperature, K
t	time, s
u	velocity, $m \cdot s^{-1}$
z	location along the axis of the tank, m

Greek

α	thermal diffusivity, $m^2 \cdot s^{-1}$
β	thermal expansion coefficient, K^{-1}
ν	kinematic viscosity, $m^2 \cdot s^{-1}$
ε	porosity of packed-bed region
μ	viscosity, $kg \cdot m^{-1}\ s^{-1}$
ρ	density, $kg \cdot m^{-3}$
Γ	effective thermal conductivity, $W \cdot m^{-1}\ K^{-1}$
ξ	radial coordinate inside each capsule

Subscripts

eff	effective value
g	air
high	high temperature
in	inlet; input
low	low temperature
l	liquid phase
m	melting
p	PCM
R	radius
s	solid phase
tank	thermal energy storage system

Abbreviations

HTF	heat transfer fluid
PCM	phase change material
TES	thermal energy storage

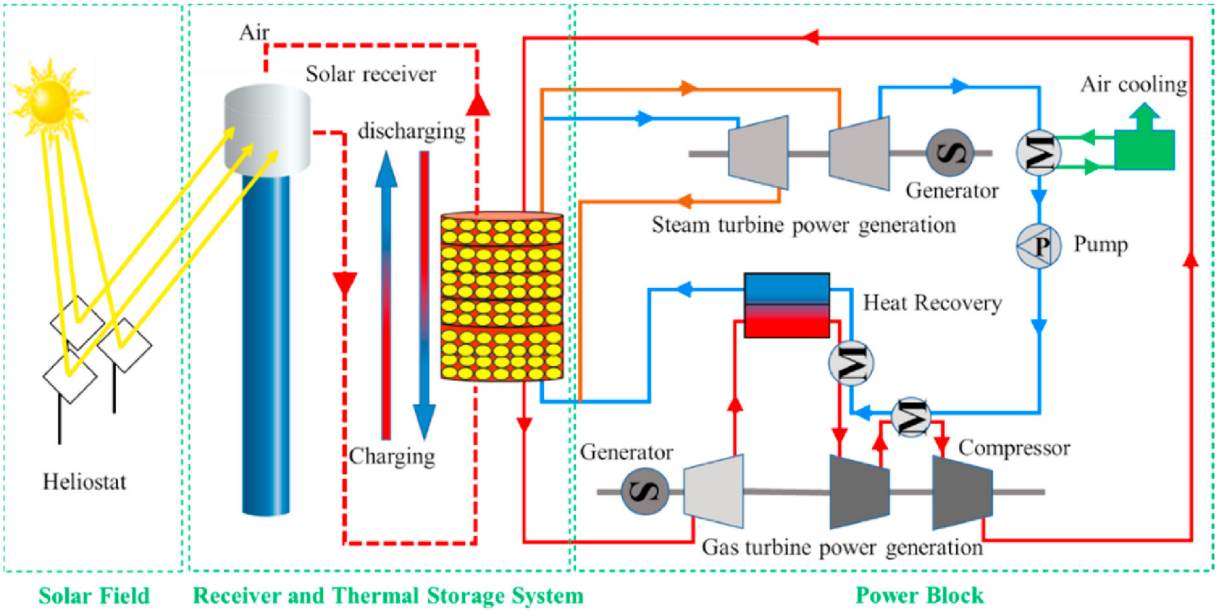

Fig. 1. Schematic layout of a concentrating solar power hybrid power plant using the packed-bed latent thermal energy storage with PCM capsules.

of heat transfer between heat transfer fluid and storage materials.

In previous studies, Ismail et al. [20] used the dispersion-concentric (D-C) scheme to study the dynamic behavior of the thermocline TES tank with PCM as storage materials. They concluded that the entry temperature of the working fluid had a dominant and strong effect on phase change behavior. Regin et al. [21] analyzed the behavior of packed bed LTES system, which was composed of spherical capsules filled with paraffin wax. Their research results showed that for the proper modeling of performance of the system the phase change temperature range of the

PCM must be accurately known, and should be taken into account. Karthikeyan et al. [22] compared three different numerical models of packed bed LTES system. Their research results indicated that mathematical models should be matched with exchange fluids because of requirements of different calculation precisions. Xu et al. [23,24] presented a transient two-dimensional D-C model to study thermal properties of a TES system that consists of molten salt packed-bed and PCM capsule fillers. Their research results found that the effective discharging efficiency of the system can be increased by decreasing the capsule diameter, decreasing the molten-salt inlet velocity or increasing the phase change temperature. Bellan et al. [25] experimentally and numerically analyzed the dynamic thermal performance of high temperature LTES system packed with spherical PCM capsules. Their research results indicated that the Stefan number plays a vital role on the total heat storage capacity due to sensible heat, and the shell properties of the capsule significantly influence the thermal performance of the system; the influence of the shell thickness increases (decreases) when the thermal conductivity of the shell was low (high). He et al. [26] proposed a new detailed cycle-to-cycle modelling framework to dynamically simulate an adiabatic compressed air energy storage system with packed bed LTES. Their time-resolved simulation results showed that a higher steady-state cycle efficiency of 56.5% for the system with the PCM-filled packed bed TES, versus 53.2% of the system with the rock-filled packed bed LTES. Liao et al. [27] developed a modified transient, one-dimensional, D-C model to investigate the dynamic performance of high temperature packed-bed LTES systems. Their research results found that for the charging/discharging cycle with cut-off temperatures, the practical system storage capacity was lower than the theoretical storage capacity, and the cut-off temperatures had great influence on the charging efficiency and the capacity ratio.

Despite great potential, packed bed LTES system has not been commercialized successfully. Early designs of packed bed LTES system used a single layered packed bed heat storage material, which greatly restricted the heat storage and release performance. To overcome these issues, multilayers packed bed structure was recently suggested to overcome the influence of thermocline on thermal performance of packed bed LTES system. Li et al. [28] have experimentally and numerically investigated the thermal performance of high temperature packed bed LTES system with macro-encapsulation of molten salt PCM. Their research results showed that the thermal resistances caused by the capsule shell were the main factor for influencing the heat transfer within the system. In addition, the authors also compared the packed bed configuration with the shell and tube configuration, and the results indicated that the thermal performance of packed bed system was better than that of shell and tube system with the overall efficiency improvement of 1.9–2.4 times. Furthermore, Authors [29] further established a new two-layered high-temperature packed-bed LTES system with changed-diameter PCM capsules, in order to improve the thermal performance of packed-bed LTES system. Their research results showed that the LTES charging rate of the two-layered packed bed TES can be improved by 12.4% compared to that of single-layered packed bed LTES, with the same inlet temperature and inlet mass flow. Mohammadnejad et al. [30] investigated the discharge performance of a packed bed filled with multi layers of high temperature encapsulated PCM through a CFD modeling. Their research results indicated that by setting the layer heights of the PCM in a descending order and also having the porosity of each layer to decrease in the flow direction, results with 29.2% better performance could be obtained. Mao et al. [31] analyzed numerically the thermal performance of a small capsule of three different PCM for a packed bed LTES system of solar energy. Their research results found that the storage capacity and utilization rate of 3-PCM energy storage systems are relatively high and the shape of the tank has no effect on the storage capacity at a fixed tank volume. Elfeky et al. [32] investigated the PCM volume fraction effect on the thermal and economic behavior of a three-layer thermocline TES tank system which is used in CSP plants. Their research results showed that the integration of three layers' thermocline tank case which has a higher volume fraction at the bottom part of the tank with CSP plants is capable of making the grid load more stable and decreasing more running fee. In summary, there have been extensive studies using different numerical approach.

1.2. Novelty and originality of this work

From the above literature review, previous research mainly focused on different PCM capsules arranged axially in the multi-layers packed bed structure to improve the thermal performance of the packed bed LTES system. To the best of the authors' knowledge, no work has been reported which focuses on the thermal performance assessment of the high-temperature LTES system using radial gradient arrangement and air as heat transfer fluid (HTF). Furthermore, for the transient two-dimensional dispersion-concentric (D-C) mode, the temperature field in porous media and the phase transition process in PCM capsules have not been studied in depth. Therefore, the main objective of this work is to investigate the thermal performance of the packed-bed LTES system using the PCM capsules with radial gradient arrangement. To study and understand the phase change process, thermo-fluid flow, charging and discharging performance in the high-temperature range, a transient two-dimensional D-C model is developed. Based on the model, the heat transfer characteristics between air and PCM capsules in four different packed-bed systems filled with PCM capsules are discussed in detailed. Both of the temperature distribution, charging time, discharging time, pressure drop, overall efficiency, capacity ratio, and utilization ratio are studied. This work can provide a design basis and numerical basis for the thermal stability output and the thermal performance optimization of packed bed latent thermal energy storage system.

2. Numerical modelling

2.1. Physical model

In this work, the design of the packed-bed LTES system is inspired by lotus root structures that exist widely in nature. Lotus roots were found buried in anaerobic sediment and are characterized by having oval holes for obtaining air [33]. Mevi-schutz and Grosse [34] conducted experiments that thermoosmotic gas transport could drive air flow from the lotus leaves to the roots. The schematic of the packed-bed LTES system and the radial gradient arrangement using PCM capsules are presented in Fig. 2. The packed-bed LTES system consists of a vertically standing cylindrical system. Adjacent to the two ports, two short distributors are installed to achieve uniform airflow through the cross-section of the packed-bed region. During the charging process, the high-temperature air enters from the top of the storage bed along the negative direction of the Z-axis. In contrast, during the discharging process, the low-temperature air enters from the bottom of the storage bed along the positive direction of the Z-axis. Inside of the system is pack with PCM capsules that have the same material. Four cases are investigated in the current study, as illustrated in Fig. 2. The porosity of the bed is the same in all cases of the charging and discharging process. Case 1 and case 2 are filled with PCM capsules with diameters of 15 mm and 25 mm, respectively. In case 3 and case 4, the tank is divided into three parts according to the radial

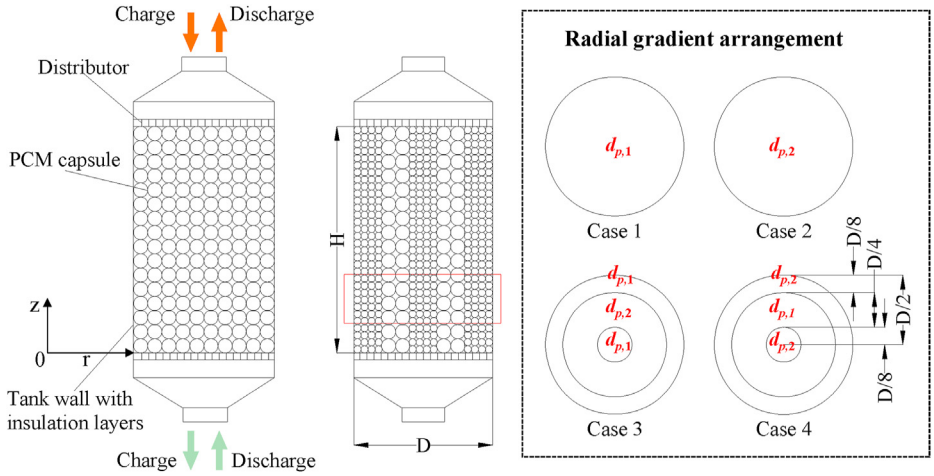

Fig. 2. Schematic illustration of the packed-bed latent thermal energy storage system using spherical PCM capsules and the computational domain.

gradient arrangement. Case 3 is fill with PCM capsules with diameters of 15 mm, 25 mm, and 15 mm. Case 4 is filled with PCM capsules with diameters of 25 mm, 15 mm, and 25 mm. The PCM capsules are ternary carbonate Li_2CO_3–K_2CO_3–Na_2CO_3 (32–35–33 wt%). The geometric parameters, the stainless steel, and the insulation layer [24], and the properties of PCM used [28] in the model are listed in Table 1.

2.2. Governing equations

To evaluate the effects of PCM capsules on the performance of the packed-bed LTES system, a transient two-dimensional D-C model is employed in this work. The D-C model treats the packed bed as an isotropic porous medium consisting of independent spherical particles [35]. Therefore, the heat transfer processes between HTF and PCM capsules and within PCM capsules can all be revealed in detailed. The following assumptions are employed in the modeling:

(1) The LTES system is symmetrical along the axis.

Table 1
Geometric parameters and properties used in the model.

Parameter	Symbol	Value	Reference
LTES system			
Height of pack-bed	m	0.50	
Diameter of pack-bed	m	0.30	
Tank wall thickness	m	0.01	
Insulation thickness	m	0.25	
Phase Change Material (Li_2CO_3–K_2CO_3–Na_2CO_3)			
Porosity	/	0.5	
Density of PCM	kg/m^3	2310.0	[28]
PCM latent heat of fusion	kJ/kg	273.0	[28]
Melting temperature of PCM	°C	395.1	[28]
Specific heat capacity for solid PCM	J/kg·K	1540.0	[28]
Specific heat capacity for liquid PCM	J/kg·K	1640.0	[28]
Thermal conductivity for solid PCM	W/m·K	1.69	[28]
Thermal conductivity for liquid PCM	W/m·K	1.60	[28]
Stainless steel and insulation layer			
Specific heat capacity for stainless steel	J/kg·K	470	[24]
Thermal conductivity for stainless steel	W/m·K	35.0	[24]
Density for stainless steel	kg/m^3	7800	[24]
Specific heat capacity for insulation layer	J/kg·K	960	[24]
Thermal conductivity for insulation layer	W/m·K	0.1	[24]
Density for insulation layer	kg/m^3	2000	[24]

(2) The PCM capsules are isotropic spherical particles with the same diameter, the porosity inside the packed bed is uniform.
(3) The volume change of PCM during the phase change process is ignored.
(4) The packed PCM capsules form a continuous, homogeneous, and isotropic porous region for fluid flow, and the flow of air through the packed-bed region is laminar and incompressible.
(5) The initial temperature of the system unit is assumed to be uniform, and the air inlet velocity and temperature are both stable during the charging process.

With these assumptions, the governing equations of transient two-dimensional D-C model are presented as follows.

Conservation of mass equation [24]:

$$\frac{\partial(\varepsilon\rho_g)}{\partial t}+\nabla\left[\rho_g\vec{u}\right]=0 \tag{1}$$

where ρ_g is the air density, and $\vec{u}=u_r\vec{e}_r+u_z\vec{e}_z$ is the superficial velocity vector based on the total cross-sectional area of packed-bed region.

Conservation of momentum equation [24]:

$$\frac{\partial(\rho_g\vec{u})}{\partial(\varepsilon t)}+\frac{\nabla\left[\rho_g\vec{u}\vec{u}\right]}{\varepsilon^2}=\nabla\cdot\left(\frac{\mu_g}{\varepsilon}\nabla\vec{u}\right)-\nabla p+\rho_g\vec{g}-\left(\frac{\mu_g}{K}+\frac{C_F\rho}{\sqrt{K}}|\vec{u}|\right)\vec{u} \tag{2}$$

where μ_g is the air viscosity, C_F is the inertial coefficient, and K is the intrinsic permeability of the porous medium.

Conservation of energy equation for air [24]:

$$\frac{\partial(\varepsilon\rho_g c_{p,g}T_g)}{\partial t}+\nabla\left[\rho_g c_{p,g}\vec{u}T_g\right]=\nabla\cdot\left(\Gamma_{g,eff}\nabla T_g\right)+h_v\left((T_p)_R-T_g\right) \tag{3}$$

where T_g is the air temperature, $(T_p)_R$ is the surface temperature of PCM capsules, $c_{p,g}$ is the specific heat capacity of air, $\Gamma_{g,eff}$ is the effective thermal conductivity of air, and the heat transfer between air and capsules is accounted for by the last term on the right side using a volumetric interstitial heat transfer coefficient h_v.

Conservation of energy equation for PCM capsules [24]:

$$\frac{\partial(\rho_p h_p(T_p))}{\partial t}=\frac{\partial}{\partial\xi}\left(k_p(T_p)\frac{\partial T_p}{\partial\xi}\right)+\frac{2k_p(T_p)}{\xi}\frac{\partial T_p}{\partial\xi} \tag{4}$$

where ξ is the radial coordinate inside each capsule, h_p is the enthalpy of PCM, ρ_p and k_p are the density and thermal conductivity of PCM, respectively.

Conservation of energy equation for the insulation layers and system steel wall [24]:

$$\frac{\partial(\rho_i c_{p,i} T_i)}{\partial t}=\nabla\cdot(\Gamma_i\nabla T_i) \tag{5}$$

where i indicates system steel wall and insulation layer.

2.3. Material properties and constitutive correlations

The thermo-physical properties of air change with temperature and can be found as follows [27]:

Density, ($kg\cdot m^{-3}$):

$$\rho_g=1.274-0.004509T_g+1.343\times10^{-5}T_g^2-2.799\times10^{-8}T_g^3 +3.56\times10^{-11}T_g^4-2.429\times10^{-14}T_g^5+6.75\times10^{-18}T_g^5 \tag{6}$$

Specific heat capacity, ($J\cdot kg^{-1}\cdot K^{-1}$):

$$c_{p,g}=1006-0.008615T_g+6.581\times10^{-4}T_g^2 -7.131\times10^{-7}T_g^3+2.42\times10^{-10}T_g^4 \tag{7}$$

Thermal conductivity, ($W\cdot m^{-1}\cdot K^{-1}$):

$$\lambda_g=0.02477+7.298\times10^{-5}T_g-2.592\times10^{-8}T_g^2 +9.381\times10^{-12}T_g^3 \tag{8}$$

Viscosity, ($kg\cdot m^{-1}\cdot s^{-1}$):

$$\mu_g=1.743\times10^{-5}+4.76\times10^{-8}T_g-2.243\times10^{-11}T_g^2 +8.118\times10^{-15}T_g^3 \tag{9}$$

In the above equations the unit of air temperature T_g is °C.

The inertial coefficient and permeability of the packed-bed porous region are given as [36]:

$$C_F=\frac{1.75}{\sqrt{150\varepsilon^3}} \tag{10}$$

$$K=\frac{d_p^2\varepsilon^3}{150(1-\varepsilon)^2} \tag{11}$$

where d_p is the diameter of PCM capsule.

From Eqs. (3) and (4), it should be noted that the above energy conservation equations of air and capsules are coupled through the interfaces between air and capsules. Hence, the heat exchange at these interfaces is calculated by Ref. [27]:

$$k_p\frac{\partial T_p}{\partial\zeta}=h_s\left(T_g-T_p|_{\xi=d_p/2}\right) \tag{12}$$

where h_s is the heat transfer coefficient at the capsule surface, $h_s = h_v(6(1-\varepsilon)/d_p)$.

The interstitial heat transfer coefficient between air and capsulesh_v, is given as [24,27]:

$$h_v=\frac{6(1-\varepsilon)k_pNu_p}{d_p^2} \tag{13}$$

where the Nusselt number, Reynolds number and Prandtl number are given as below:

$$Nu_p=2+1.1\mathrm{Re}_p^{0.6}\mathrm{Pr}^{1/3};\ \mathrm{Re}_p=\frac{\rho_g d_p|\vec{u}|}{\mu};\ \mathrm{Pr}=\frac{c_{p,g}\mu}{k_g} \tag{14}$$

When the PCM is in liquid phase, natural convection may occur which enhances the heat transfer. The natural convection effect of the liquid PCM is taken into account by using the following effective thermal conductivity of liquid PCM [24]:

$$k_{p,conv}=0.18k_pRa^{0.25} \tag{15}$$

$$Ra=g\beta(T_p-T_{melt})(d_p/2)^3\Big/\nu\alpha \tag{16}$$

where ν, α and β are the kinematic viscosity, thermal diffusivity, and thermal expansion coefficient, respectively.

For the packed bed mode, the equivalent thermal conductivity of air is based on the following equation [37]:

$$\Gamma_{g,eff}=k_g\left[\frac{1+2\beta\varphi+(2\beta^3-0.1\beta)\varphi^2+\varphi^3 0.05\exp(4.5\beta)}{1-\beta\varphi}\right] \tag{17}$$

where $\varphi=1-\varepsilon$, $\beta=(k_p-k_g)/(k_p+2k_g)$.

When air is used as the HTF, pumping power requirements can be substantial. Therefore, a commonly employed pressure drop equation for the packed bed is determined to be the following [31]:

$$\frac{\Delta P}{H}=150\frac{(1-\varepsilon)^2}{\varepsilon^2}\frac{\mu_g\vec{u}}{d_p^2}+1.75\frac{1-\varepsilon}{\varepsilon^3}\frac{\rho_g\vec{u}^2}{d_p} \tag{18}$$

The phase change of PCM is occurred during the charging and discharging process and physical parameters are changed relatively. The effective heat capacity method is adopted to properly describe it. The method regards the phase change is resulted within a small temperature interval ($\Delta T_m = T_{m2}-T_{m1}$), and PCM has a large specific heat capacity within it. Three stages of the charging process and the discharging process as presented as below.

The solid sensible heating period is expressed as:

$$\begin{cases}c_p=c_{p,s}\\ k_p=k_s\end{cases},\ T_p<T_{m1} \tag{19}$$

The phase change thermal storage period is presented as:

$$\begin{cases}c_p=\dfrac{c_{p,l}+c_{p,s}}{2}+\dfrac{L}{T_{m2}-T_{m1}}=\dfrac{c_{p,l}+c_{p,s}}{2}+\dfrac{L}{\Delta T_m}\\ k_p=\dfrac{k_s+k_g}{2}\end{cases},\ T_{m1}<T_p<T_{m2} \tag{20}$$

The liquid sensible heating period is formulated as:

$$\begin{cases}c_p=c_{p,l}\\ k_p=k_l\end{cases},\ T_p>T_{m2} \tag{21}$$

2.4. Boundary conditions and initial conditions

In this study, various working processes are simulated including the charging and discharging processes. In the charging process, the initial temperature of packed bed is 298.15 K, and the inlet temperature is 773.15 K. In the discharging process, the initial temperature of packed bed is 773.15 K, and the inlet temperature is 298.15 K. The mass flow rate is 220 kg/h. The boundary conditions of the air for the different working processes are expressed as follows.

The charging process:

$$z=0:\partial u/\partial z|_{+}=0,\partial T_g/\partial z|_{+}=0 \tag{22}$$

$$z=H:u|_{-}=-u_{in},T_g|_{-}=T_{in,high} \tag{23}$$

The discharging process:

$$z=0:u|_{+}=u_{in},T_g|_{+}=T_{in,low} \tag{24}$$

$$z=H:\partial u/\partial z|_{-}=0,\partial T_g/\partial z|_{-}=0 \tag{25}$$

Convective heat flux boundary condition is given:

The total heat transfer coefficient is determined by the heat transfer resistance between the HTF and the system wall as below:

$$\frac{1}{h_w}=\frac{1}{h_i}+r_{bed}\sum_{k_j}^{n}\frac{1}{k_j}\ln\left(\frac{r_{j+1}}{r_j}\right) \tag{26}$$

The inner wall heat loss coefficient is given as follows:

$$h_i=\frac{k_g}{d_p}\left[\left(0.203\mathrm{Re}^{1/3}\mathrm{Pr}^{1/3}\right)+\left(0.22\mathrm{Re}^{0.8}\mathrm{Pr}^{0.4}\right)\right] \tag{27}$$

3. Model validation

To validate the correctness of the numerical model, the difference between numerically predicted results and literature results for the charging and discharging processes of packed bed LTES system is inspected [28], as shown in Fig. 3. Air is used as the heat transfer fluid, the mass flow rate is 260 kg/h, the diameter of the PCM particles is 34 mm, and the porosity is 0.426. A comparison of simulation and literature results shows that, the average deviations in the charging processes and the discharging processes are approximately 8.7% and 9.3%, respectively. The results indicate that the predictions from the present model agree well with the results, which confirms that the present transient two-dimensional D-C model can provide reasonable predictions.

4. Results and discussion

4.1. The temperature evolution of the charging process

The charging characteristics of the four LTES systems are discussed in this section. Each tank is assumed to be fully discharged at the beginning. The temperature evolution of PCM capsules and HTF at the central of the axial and the radial during the charging process in four different cases are shown in Fig. 4. As can be seen, the PCM underwent a solid-state sensible heat storage period, a phase changes latent heat period, and a liquid-state sensible heat storage period. As can be seen from Fig. 4(a), the time when the temperature of PCM capsules and the temperature of HTF reach the highest temperature is case 1, case 3, case 4, and case 2, respectively. As can be seen from Fig. 4(b), the time when the temperature of PCM capsules and the temperature of HTF reach the highest temperature is case 3, case 1, case 2, and case 4, respectively. The main reason for this phenomenon is that the smaller the diameter of PCM capsules, the shorter the time for the PCM capsules to reach the maximum temperature, as shown in case 1 and case 2 in the figure. However, by comparing case 2 and case 4, it can be found that, because case 4 adopts smaller diameter of PCM capsules in the radial position, the heat transfer process in the axial region is increased, resulting in a shorter heat storage time in case 4. By comparing case 1 and case 3, it also can be found that case 3 uses larger diameter of PCM capsules in the radial position, so the heat transfer process in the axial region is reduced, leading to longer heat storage time in case 3.

To better analyze the heat transfer relationship between HTF and PCM capsules, the evolution of temperature difference between HTF and PCM is adopted to investigate further, as shown in Fig. 5. It can be seen that there are two peaks happened in the temperature difference between HTF and PCM in four different cases. In the stage of solid sensible heat, the temperature difference of the PCM gradually increased and reached the maximum point. The first peak point appears the medial stage of solid sensible heat. The maximum temperature difference between HTF and PCM from case 1 to case 4 is 41.07 K, 62.80 K, 39.21 K, 65.28 K, respectively. Then the temperature difference became smaller, with the temperature of the PCM increased gradually. The trough point appears at the beginning of the melt. In the stage of phase change latent heat, because of the slow increasing speed of the PCM during the

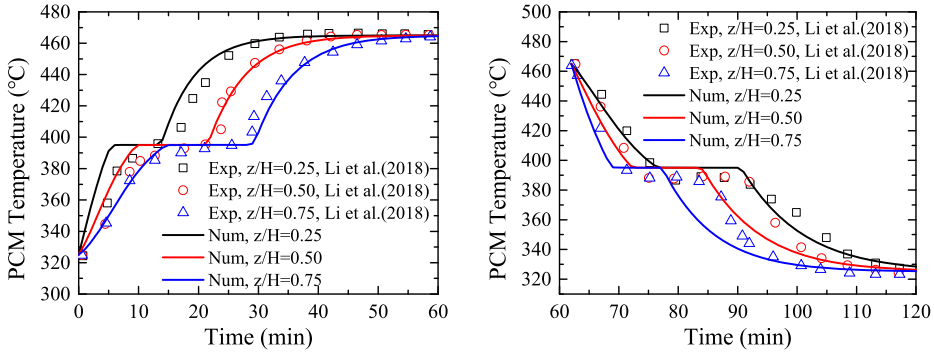

Fig. 3. Comparison between current numerical result and literature results [28].

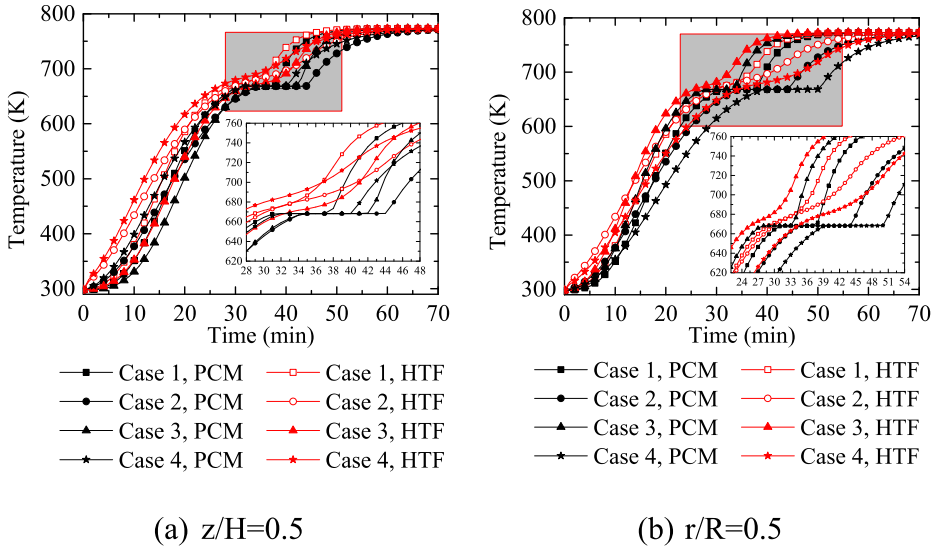

Fig. 4. Temperature evolution of air and PCM capsules during the charging process in four different cases, (a) z/H = 0.5, (b) r/R = 0.5.

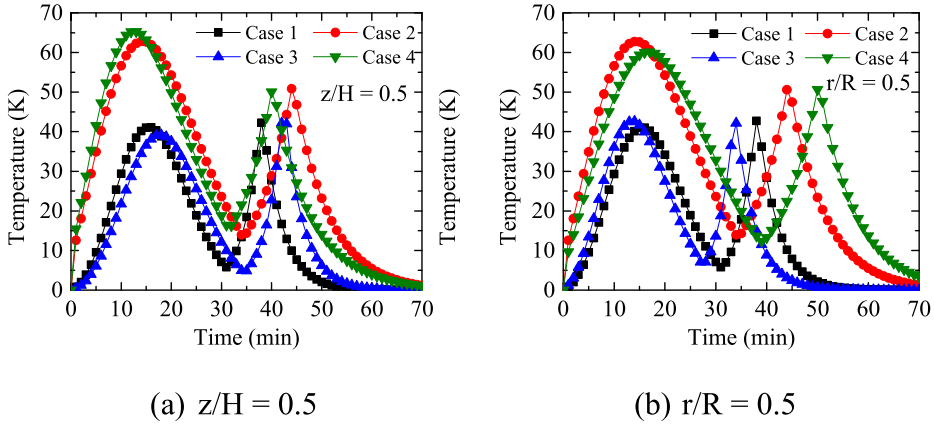

Fig. 5. Temperature difference between air and PCM capsules during the charging process in four different cases, (a) z/H = 0.5, (b) r/R = 0.5.

melting process, the temperature difference is larger again and arrived at the second peak point. The second peak point appears at the end stage of phase change latent heat. The maximum temperature difference between HTF and PCM arrived at 50 K and then dropped. In the stage of liquid sensible heat, the temperature difference decreased gradually to 0 with the rise in temperature of the PCM until the end of the charging process. Furthermore, by comparing case 1 (or case 3) with case 2 (or case 4), it can be found that the larger temperature difference is caused by the greater diameters. The main reason for this phenomenon is that the thermal resistance of convection heat transfer between PCM capsules and HTF is the main factor affecting the entire heat exchange process, which is analyzed according to Formula 12. Therefore, the larger the PCM capsules diameter, the greater the thermal resistance of convection heat transfer that leads the longer charging process.

The temperature evolution trends of the HTF along the central axial direction during the charging process in four different cases are shown in Fig. 6. The results show that an apparent temperature difference between the top part and the bottom part of the bed at the beginning of the charging process. The reason is that the PCM will absorb heat and then melt when the HTF through the packed bed. Consequently, the temperature of HTF will gradually decrease along the fluid flow direction. Moreover, the temperature of the PCM increases sharply and the temperature of the HTF decreases sharply along the axial direction at the beginning of the charging process, because the heat transfer rate between the high-temperature air and PCM is high due to the large temperature difference.

The D-C model treats the packed bed as an isotropic porous medium consisting of independent spherical particles. Therefore, the temperature distribution contour and liquid fraction contour in four different cases at 25 min during the charging process are shown in Fig. 7. The symmetry of the geometry of the bed, to save calculation time, only half of the bed has been presented. It is found that a non-uniform distribution of the size of the capsules influences the radial distribution of the flow rate and consequently influences the temperature distribution. One can clearly see that the thermocline region is moving upward with the larger diameter of PCM capsules, accompanied by slight expansion. The outlet temperature evolution of HTF and the average liquid fraction of PCM capsules during the charging process are shown in Fig. 8. When the temperature of the heat storage system reaches 768 K, it means that the heat storage system is full. From case 1 to case 4, the storage end time of the system is 85 min, 104 min, 100 min, and 101 min, respectively. The smaller diameter of PCM capsules, the higher the proportional increase in energy storage, which shows

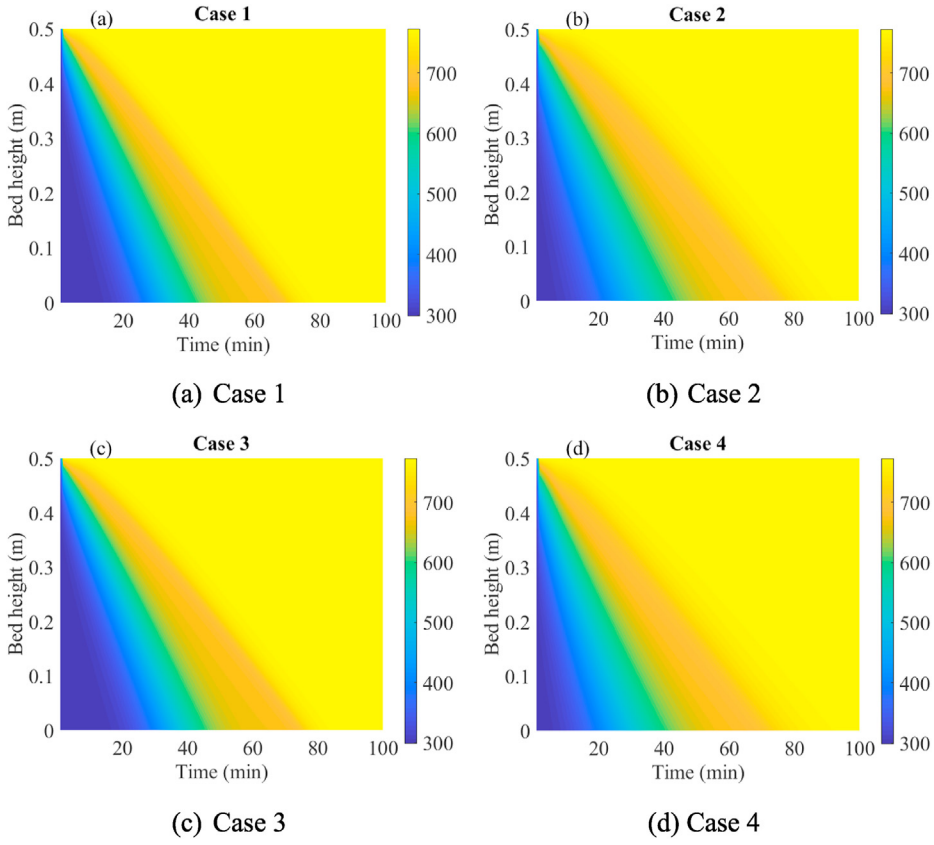

Fig. 6. Temperature evolution trends of air along the central axial direction during the charging process in four different cases.

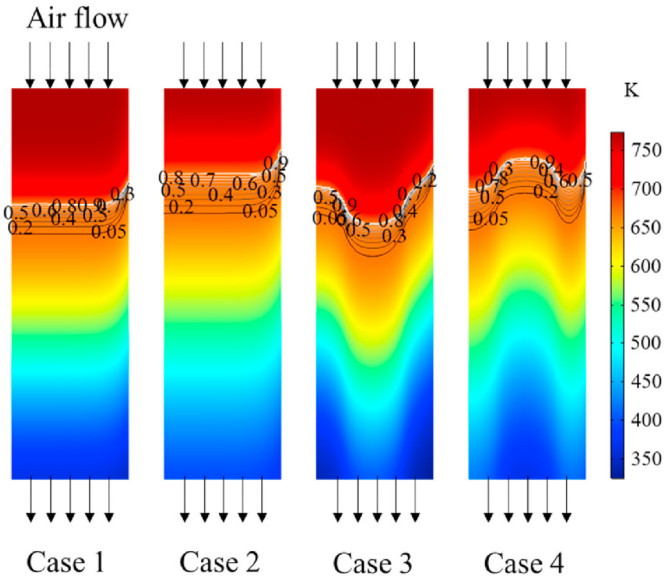

Fig. 7. Temperature distribution contour and liquid fraction contour at 25 min during the charging process in four different cases.

that the initial rise of outlet temperature is slower, and the subsequent increase in outlet temperature is rapid. It is also found that the smaller diameter of PCM capsules, the shorter the time required to complete the energy storage. However, it should be noticed that the smaller diameter of PCM capsules will increase the total manufacturing costs, and the pressure drop as well.

4.2. The temperature evolution of the discharging process

The single discharging processes of the four LTES systems are investigated in the following section. Each tank is assumed to be fully charged at the beginning. The temperature evolution of PCM capsules and HTF at the center of the axial and the radial during the discharging process in four different cases are shown in Fig. 9. As can be seen, the temperature of the air is higher than the temperature of PCM during the charging process, and the temperature of PCM is higher than the temperature of HTF during the discharging process. Fig. 10 shows the evolution of temperature difference between HTF and PCM during the discharging process, $z/H = 0.5$, and $r/R = 0.5$. There are two peaks happened in the temperature difference between PCM and HTF in four different cases. The maximum peak point occurred at the end of the phase change latent heat stage, and the maximum temperature difference between the HTF and the PCM from case 1 to case 4 is 77.55 K, 98.57 K, 78.70 K, 100.44 K, respectively. Furthermore, case 1 shows that the maximum temperature difference in the charging process is 41.07 K, and the maximum temperature difference in the discharging process is 77.55 K. It can also be found that the temperature difference between HTF and PCM increases rapidly in the stage of phase change latent heat. In summary, to improve the heat transfer performance between HTF and PCM, the smaller diameter of PCM and the radial gradient arrangement can be adopted.

The temperature evolution trends of air along the central axial direction during the discharging process in four different cases are shown in Fig. 11. From the temperature field of air, and it can be found that the temperature of air increases gradually along the axial direction of the system during the discharging process. Meanwhile, it is also observed that the time taken to cross the

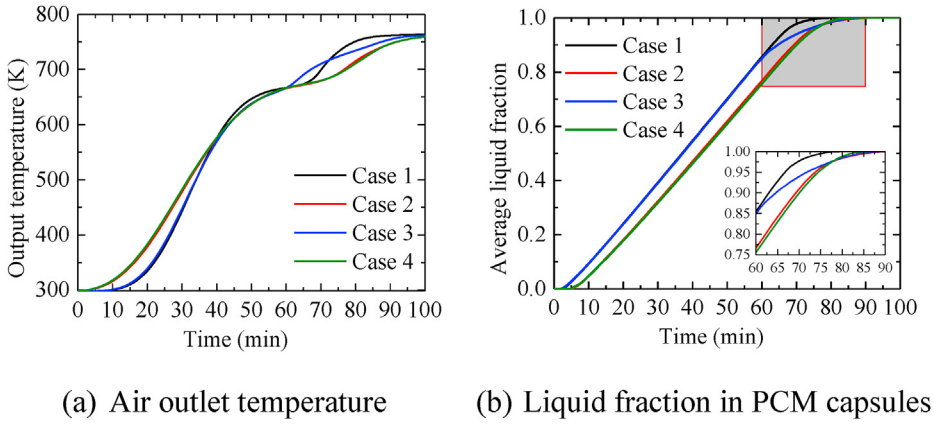

Fig. 8. Outlet temperature evolution of air and liquid fraction of PCM capsules during the charging process in four different cases.

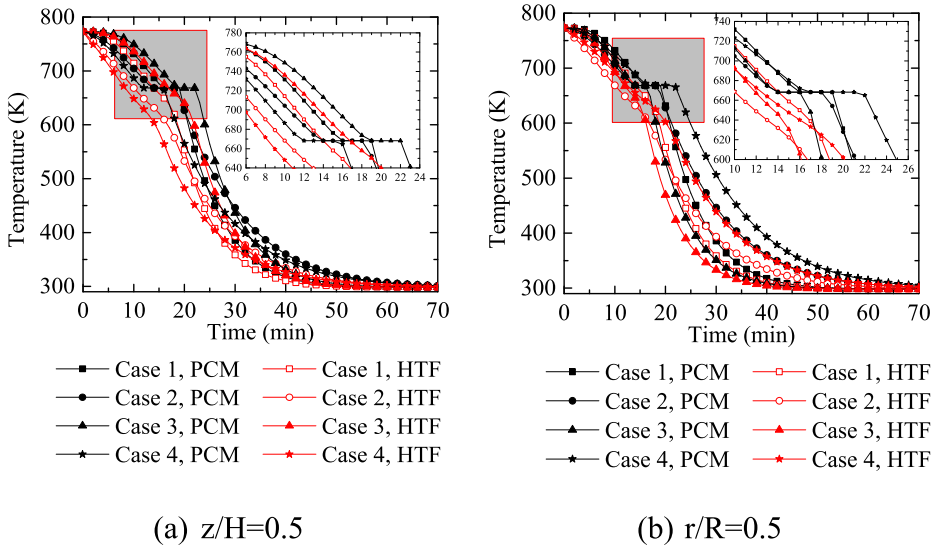

Fig. 9. Temperature evolution of air and PCM capsules during the discharging process in four different cases, (a) z/H = 0.5, (b) r/R = 0.5.

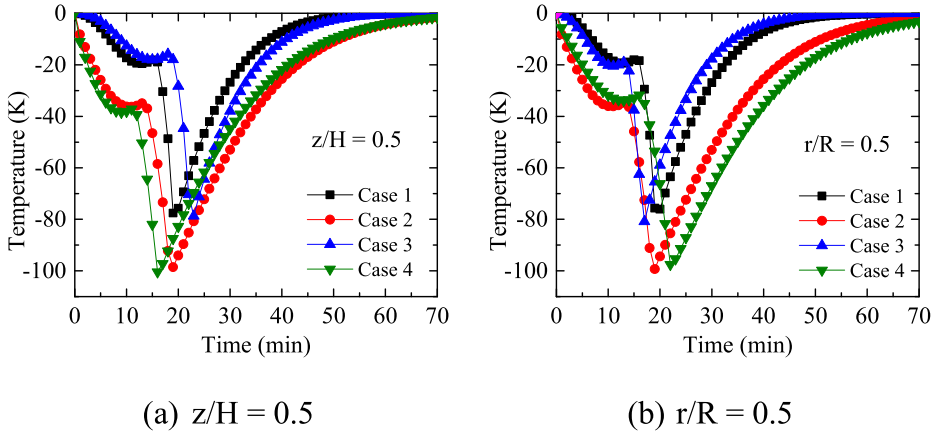

Fig. 10. Temperature difference between air and PCM capsules during the discharging process in four different cases, (a) z/H = 0.5, (b) r/R = 0.5.

phase change latent heat stage during the discharging process is faster than the charging process.

To better analyze the heat transfer relationship between HTF and PCM capsules during the discharging process, the temperature distribution contour and liquid fraction contour in four different cases at 25 min during the discharging process are shown in Fig. 12. It is seen that the smaller the diameter of PCM capsules, the wider the thermocline region and longer the phase transition time. The

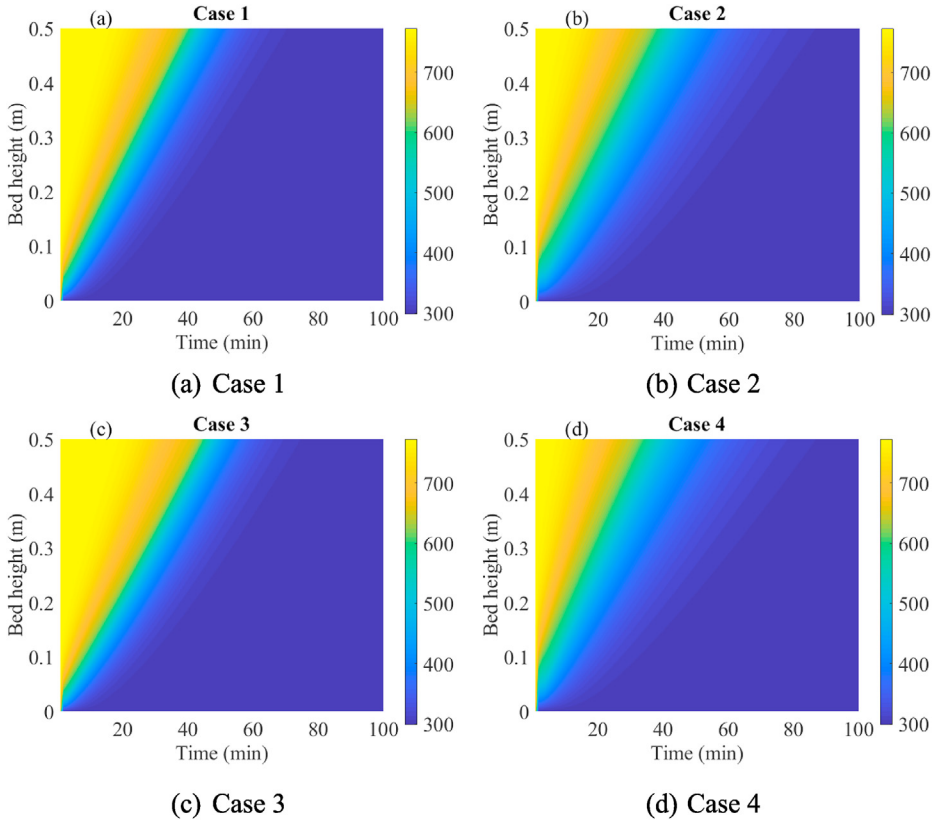

Fig. 11. Temperature evolution trends of air along the central axial direction during the discharging process in four different cases.

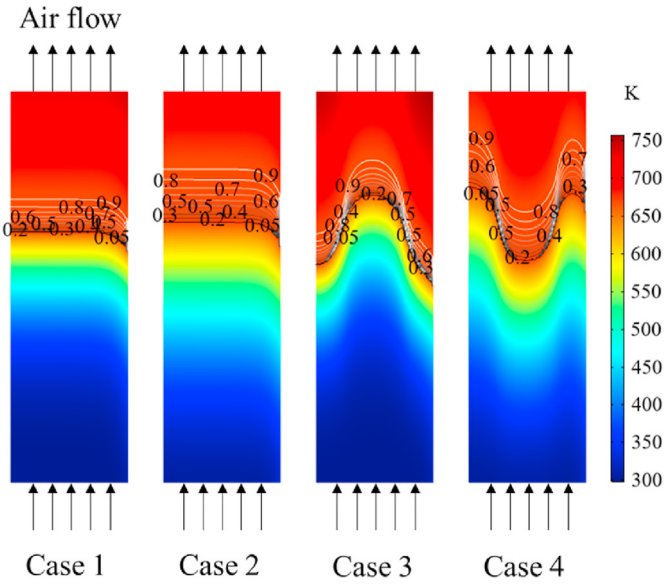

Fig. 12. Temperature distribution contour and liquid fraction contour at 25 min during the discharging process in four different cases.

reason is that the thermal resistance of the PCM inside of capsules increases with the larger diameter of capsules. The outlet temperature evolution of the HTF and the liquid fraction of PCM capsules during the discharging process are shown in Fig. 13. When the temperature of the TES system reaches 320 K, it means that the discharging process ends. It is observed that the time taken to cross the heat transfer stage during the discharging process is faster than the charging process. From case 1 to case 4, the release end time of the system is 70 min, 84 min, 75 min, and 84 min, respectively. It can be seen from Fig. 12 that case 2 and case 4 provides a relatively constant heat transfer flow in the HTF flow direction. Generally, in CSP plants, the HTF leaving the system during the discharging process is fed into the power block for superheated steam generation. Since the power block cycle process depends on the HTF temperature, it requires the termination of the discharging process when the HTF outlet temperature reaches the minimum cut-off temperature [38]. Thus, a faster rate of discharging leads to lower performance time for a CSP system, which is undesirable. The results indicate that there is no need to have the HTF completely drain the energy of spheres of the PCM, but it is only needed to raise the temperature of the HTF to the point that is necessary. By doing so, HTF with the desired temperature can be obtained for a longer time.

4.3. Performance analysis

In the performance analysis part, the overall energy efficiency and capacity ratio and utilization ratio have been utilized to evaluate the thermal performance of the packed bed LTES system [39], as shown in Table 2. The quantity of the storage energy in the packed bed LTES system is changing and dependent on the radial gradient arrangement of PCM capsules. From Table 2, the result show that the capacity ratio of case 1 is higher than all studied cases by 5.03%, 1.11%, and 3.74%, respectively. Moreover, the also result show that the utilization ratio of case 1 is higher than all studied cases by 5.15%, 1.45%, and 3.43%, respectively. From case 1 to case 4, the overall energy efficiency of the system is 84.16%, 80.43%, 83.55%, and 82.46%, respectively. Therefore, it can be found that the overall energy efficiency of case 1 and case 3 is higher, and the efficiency of

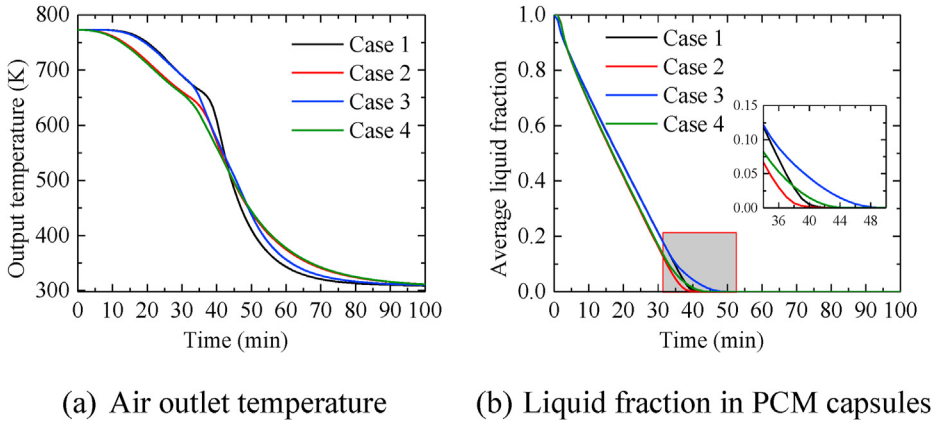

Fig. 13. Outlet temperature evolution of air and liquid fraction of PCM capsules during the discharging process in four different cases.

Table 2
Thermal performance of the packed bed latent thermal energy storage system in four different cases.

Performance parameter	Case 1	Case 2	Case 3	Case 4
Charging/Discharging time (min)	85/70	104/84	100/75	101/84
Overall energy efficiency (%)	84.16	80.43	83.55	82.46
Capacity ratio (%)	86.32	81.29	85.21	82.58
Utilization ratio (%)	85.62	80.47	84.17	82.19

case 2 and case 4 is lower. To elaborate the better thermal performance of packed bed LTES, this study compares the results with the literature [40]. It can be summarized that the thermal performance of packed bed LTES is greater than that of shell and tube thermal storage system and a finned-tube thermal storage system after the comparison. Furthermore, this study further compares the results with the literature [28]. Comparing case 1 with the results in the literature, it can be found that the overall energy efficiency is greater. The main reason is that a smaller diameter of PCM capsules is used in this work.

The aim of studying packed beds during the discharging process is to increase the duration of recovering energy with the desired temperature. To better compare the thermal performance of each case, total energy utilization is used in this part [30]. The total energy utilization during the discharging process in four different cases is analyzed, as shown in Fig. 14. It can be seen that the higher the temperature requirement, the shorter the discharging time and the lower the total energy utilization. The results showed that when the demand temperature is 350K, the total energy utilization from Case 1 to Case 4 is 58.0%, 66.5%, 61.0%, 67.0%, respectively; when the demand temperature is 750K, the total energy utilization from Case 1 to Case 4 is 20.0%, 13.5%, 19.0%, 12.5%, respectively. Therefore, it can be found that different temperature requirements with different radial gradient distribution of PCM, can get better performance. In the high-temperature stage, the total energy utilization of case 1 is 20%, which is 7%, 1%, and 7.5% higher than Case 2, Case 3, and Case 4, respectively. In the low-temperature stage, the total energy utilization of case 4 is 67%, which is 9%, 0.5%, and 6% higher than Case 1, Case 2, and Case 3, respectively. Only by making little changes in the packed bed radial gradient arrangement and without any need to change the PCM, it is possible to help enhance the total energy utilization of the discharging process.

Formula 18 indicates that the pressure drop decreases as the diameter of PCM capsules increases; thus, the diameter of PCM capsules would be ideal if the goal is to minimize the pumping requirement. However, the increase in convective heat transfer must be balanced against the associated increase in pressure drop across the packed bed. The pressure drop changes between the outlet and the inlet are shown in Fig. 15. Moreover, it also can be seen that the pressure drops of case 1 increases from 151.49 Pa to 387.42 Pa, the pressure drops of case 2 increases from 86.36 Pa to 225.39 Pa, the pressure drops of case 3 increases from 114.54 Pa to 296.55 Pa, and the pressure drops of case 2 increases from 109.47 Pa to 281.20 Pa when the input mass flow rate increases from 180 kg/h

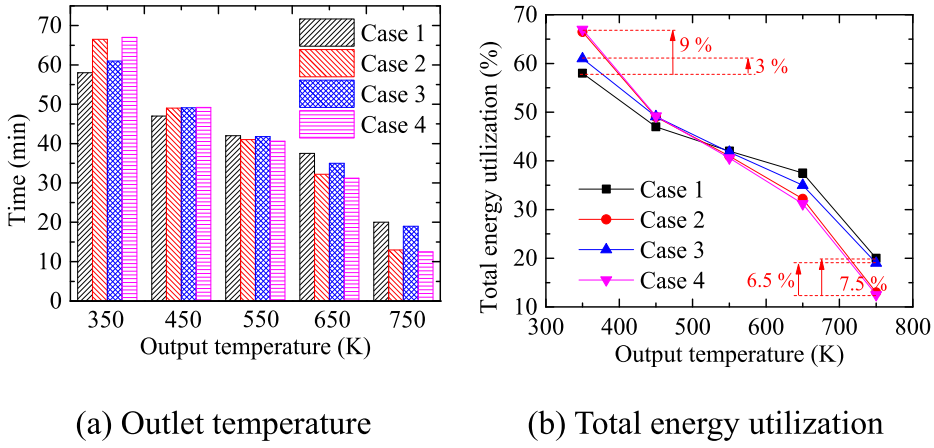

Fig. 14. Total energy utilization during the discharging process.

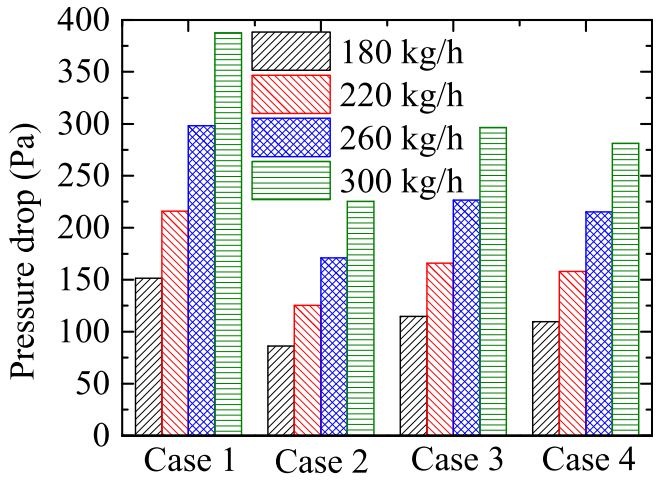

Fig. 15. Pressure drops changes in four different cases.

to 300 kg/h. Since the pressure drop increases when increasing the flow rate, the fully charged or discharged time of the system decreases. To sum up, the radial gradient arrangement should be used to reduce the pressure drop of the TES system. In the above comparative study, considering the loss of pressure drop, the results indicate that case 3 is the most viable option of all the studied cases. These investigations can help better and more efficiently utilize PCM packed beds and reach better performances in thermal cascade utilization and efficient and stable thermal output in the future.

5. Conclusions

The main objective of this work is to investigate the influence of phase change material capsules using radial gradient arrangement on the thermal performance of the packed bed latent heat storage system. First, the transient two-dimensional dispersion-concentric model is developed and validated. With the use of this model, the heat transfer between air and phase change material capsules and the phase change process within capsules are analyzed. Moreover, the temperature distribution and the thermal performance of the charging and discharging processes of four different arrangements are compared. Finally, this work also considers the influence of phase change material radial gradient arrangement on the charging time, discharging time, pressure drop, overall efficiency, capacity ratio and utilization ratio of the system. The following conclusions from the current work are summarized:

(1) The thermal resistance of convection heat transfer between phase change materials capsules and air is the main factor affecting the entire heat exchange process. The larger the diameter of phase change material capsules, the greater the thermal resistance of convection heat transfer. To improve the heat transfer performance between air and phase change materials, the smaller diameter of phase change materials or the radial gradient arrangement can be adopted.

(2) The smaller the diameter of phase change material capsules, the shorter the time for the phase change materials to reach the maximum temperature, and the shorter the time required to complete the energy storage, while the thermal efficiency is higher. The increase in convective heat transfer must be balanced with the increase in pressure drop across the packed bed. The radial gradient arrangement should be used to reduce the pressure drop.

(3) From case 1 to case 4, the overall energy efficiency of the system is 84.16%, 80.43%, 83.55%, and 82.46%, respectively. The capacity ratio of case 1 is higher than all studied cases by 5.03%, 1.11%, and 3.74%, respectively. Moreover, the also result shows that the utilization ratio of case 1 is higher than all studied cases by 5.15%, 1.45%, and 3.43%, respectively.

(4) Only by making little changes in the packed bed radial gradient arrangement and without any need to change the phase change materials, it is possible to help enhance the total energy utilization of the discharging process. In the above comparative study, considering the loss of pressure drop, the results indicate that case 3 is the most viable option of all the studied cases.

In the further, the authors hope to continue this work by providing a more detailed dynamic simulation model, including a concentrating solar power model or a waste heat recovery system model. It provides a design basis and numerical basis for the thermal stability output and the thermal performance optimization of high temperature latent thermal energy storage system.

CRediT authorship contribution statement

Wei Wang: Conceptualization, Formal analysis, Writing – original draft, Writing – review & editing. **Xibo He:** Methodology, Validation. **Yicheng Hou:** Formal analysis, Data curation. **Jun Qiu:** Investigation. **Dongmei Han:** Resources, Supervision, Funding acquisition. **Yong Shuai:** Project administration, Supervision, Funding acquisition.

Declaration of competing interest

The authors declare that they have no known competing financial interests or personal relationships that could have appeared to influence the work reported in this paper.

Acknowledgements

This work was supported by the China National Key Research and Development Plan Project (grant numbers: 2018YFA0702300).

References

[1] W. Wang, M. Li, Solar air heating system, in: R. Wang, X. Zhai (Eds.), Handbook of Energy Systems in Green Buildings, Springer Berlin Heidelberg, Berlin, Heidelberg, 2018, pp. 257–299.
[2] W. Wang, M. Li, R.H.E. Hassanien, Y. Wang, L. Yang, Thermal performance of indirect forced convection solar dryer and kinetics analysis of mango, Appl. Therm. Eng. 134 (2018) 310–321.
[3] A. Herez, H. El Hage, T. Lemenand, M. Ramadan, M. Khaled, Review on photovoltaic/thermal hybrid solar collectors: classifications, applications and new systems, Sol. Energy 207 (2020) 1321–1347.
[4] N. Soudi, S. Nanayakkara, N.M.S. Jahed, S. Naahidi, Rise of nature-inspired solar photovoltaic energy convertors, Sol. Energy 208 (2020) 31–45.
[5] A. Mustafa, B.G. Lougou, Y. Shuai, Z. Wang, H. Tan, Current technology development for CO2 utilization into solar fuels and chemicals: a review, Journal of Energy Chemistry 49 (2020) 96–123.
[6] Y. Shuai, B. Guene Lougou, H. Zhang, J. Zhao, C. Ahouannou, H. Tan, Heat transfer analysis of solar-driven high-temperature thermochemical reactor using NiFe-Aluminate RPCs, Int. J. Hydrogen Energy 46 (16) (2021) 10104–10118.
[7] Z.H. Wang, A. Roffey, R. Losantos, A. Lennartson, M. Jevric, A.U. Petersen, M. Quant, A. Dreos, X. Wen, D. Sampedro, K. Borjesson, K. Moth-Poulsen, Macroscopic heat release in a molecular solar thermal energy storage system, Energy Environ. Sci. 12 (1) (2019) 187–193.
[8] V. Kashyap, S. Sakunkaewkasem, P. Jafari, M. Nazari, B. Eslami, S. Nazifi, P. Irajizad, M.D. Marquez, T.R. Lee, H. Ghasemi, Full spectrum solar thermal energy harvesting and storage by a molecular and phase-change hybrid material, Joule 3 (12) (2019) 3100–3111.
[9] U. Pelay, L.A. Lu, Y.L. Fan, D. Stitou, M. Rood, Thermal energy storage systems for concentrated solar power plants, Renew. Sustain. Energy Rev. 79 (2017)

82–100.
[10] M. Liu, N.H.S. Tay, S. Bell, M. Belusko, R. Jacob, G. Will, W. Saman, F. Bruno, Review on concentrating solar power plants and new developments in high temperature thermal energy storage technologies, Renew. Sustain. Energy Rev. 53 (2016) 1411–1432.
[11] W. Wang, M. Li, H.E. Hassanien, M.E. Ji, Z.K. Feng, Optimization of thermal performance of the parabolic trough solar collector systems based on GA-BP neural network model, Int. J. Green Energy 14 (10) (2017) 819–830.
[12] G. Alva, L.K. Liu, X. Huang, G.Y. Fang, Thermal energy storage materials and systems for solar energy applications, Renew. Sustain. Energy Rev. 68 (2017) 693–706.
[13] A. Palacios, C. Barreneche, M.E. Navarro, Y. Ding, Thermal energy storage technologies for concentrated solar power – a review from a materials perspective, Renew. Energy 156 (2020) 1244–1265.
[14] J.M. Mahdi, S. Lohrasbi, E.C. Nsofor, Hybrid heat transfer enhancement for latent-heat thermal energy storage systems: a review, Int. J. Heat Mass Tran. 137 (2019) 630–649.
[15] Y.X. Lin, G. Alva, G.Y. Fang, Review on thermal performances and applications of thermal energy storage systems with inorganic phase change materials, Energy 165 (2018) 685–708.
[16] D.M. Han, B.G. Lougou, Y.T. Xu, Y. Shuai, X. Huang, Thermal properties characterization of chloride salts/nanoparticles composite phase change material for high-temperature thermal energy storage, Appl. Energy 264 (2020) 114674.
[17] W. Wang, Y. Shuai, B. Guene Lougou, B. Jiang, Thermal performance analysis of free-falling solar particle receiver and heat transfer modelling of multiple particles, Appl. Therm. Eng. 187 (2021).
[18] A. Gautam, R.P. Saini, A review on technical, applications and economic aspect of packed bed solar thermal energy storage system, Journal of Energy Storage 27 (2020) 101046.
[19] M.J. Li, Y. Qiu, M.J. Li, Cyclic thermal performance analysis of a traditional Single-Layered and of a novel Multi-Layered Packed-Bed molten salt Thermocline Tank, Renew. Energy 118 (2018) 565–578.
[20] K.A.R. Ismail, J.R. Henriquez, Numerical and experimental study of spherical capsules packed bed latent heat storage system, Appl. Therm. Eng. 22 (15) (2002) 1705–1716.
[21] A. Felix Regin, S.C. Solanki, J.S. Saini, An analysis of a packed bed latent heat thermal energy storage system using PCM capsules: numerical investigation, Renew. Energy 34 (7) (2009) 1765–1773.
[22] S. Karthikeyan, R. Velraj, Numerical investigation of packed bed storage unit filled with PCM encapsulated spherical containers – a comparison between various mathematical models, Int. J. Therm. Sci. 60 (2012) 153–160.
[23] C. Xu, X. Li, Z. Wang, Y. He, F. Bai, Effects of solid particle properties on the thermal performance of a packed-bed molten-salt thermocline thermal storage system, Appl. Therm. Eng. 57 (1–2) (2013) 69–80.
[24] M. Wu, C. Xu, Y.L. He, Dynamic thermal performance analysis of a molten-salt packed-bed thermal energy storage system using PCM capsules, Appl. Energy 121 (2014) 184–195.
[25] S. Bellan, T.E. Alam, J. Gonzalez-Aguilar, M. Romero, M.M. Rahman, D.Y. Goswami, E.K. Stefanakos, Numerical and experimental studies on heat transfer characteristics of thermal energy storage system packed with molten salt PCM capsules, Appl. Therm. Eng. 90 (2015) 970–979.
[26] W. He, J.H. Wang, Y. Wang, Y.L. Ding, H.S. Chen, Y.T. Wu, S. Garvey, Study of cycle-to-cycle dynamic characteristics of adiabatic compressed air energy storage using packed bed thermal energy storage, Energy 141 (2017) 2120–2134.
[27] Z.R. Liao, G.K. Zhao, C. Xu, C.Y. Yang, Y. Jin, X. Ju, X.Z. Du, Efficiency analyses of high temperature thermal energy storage systems of rocks only and rock-PCM capsule combination, Sol. Energy 162 (2018) 153–164.
[28] M.J. Li, B. Jin, Z. Ma, F. Yuan, Experimental and numerical study on the performance of a new high-temperature packed-bed thermal energy storage system with macroencapsulation of molten salt phase change material, Appl. Energy 221 (2018) 1–15.
[29] M.J. Li, B. Jin, J.J. Yan, Z. Ma, M.J. Li, Numerical and Experimental study on the performance of a new two-layered high-temperature packed-bed thermal energy storage system with changed-diameter macro-encapsulation capsule, Appl. Therm. Eng. 142 (2018) 830–845.
[30] F. Mohammadnejad, S. Hossainpo, A CFD modeling and investigation of a packed bed of high temperature phase change materials (PCMs) with different layer configurations, Journal of Energy Storage 28 (2020) 101209.
[31] Q.J. Mao, Y.M. Zhang, Thermal energy storage performance of a three-PCM cascade tank in a high-temperature packed bed system, Renew. Energy 152 (2020) 110–119.
[32] K.E. Elfeky, A.G. Mohammed, N. Ahmed, L. Lu, Q.W. Wang, Thermal and economic evaluation of phase change material volume fraction for thermocline tank used in concentrating solar power plants, Appl. Energy 267 (2020).
[33] Y. Zhu, C.J. Wang, D. Mynors, Applications and engineering analysis of Lotus roots under external water pressure, Appl. Bionics Biomechanics 2016 (2016) 2386982.
[34] J. Mevischutz, W. Grosse, The importance of water-vapor for the circulating air-flow through nelumbo-nucifera, J. Exp. Bot. 39 (206) (1988) 1231–1236.
[35] L. Xia, P. Zhang, R.Z. Wang, Numerical heat transfer analysis of the packed bed latent heat storage system based on an effective packed bed model, Energy 35 (5) (2010) 2022–2032.
[36] C. Xu, Z.F. Wang, Y.L. He, X. Li, F.W. Bai, Sensitivity analysis of the numerical study on the thermal performance of a packed-bed molten salt thermocline thermal storage system, Appl. Energy 92 (2012) 65–75.
[37] E.E. Gonzo, Estimating correlations for the effective thermal conductivity of granular materials, Chem. Eng. J. 90 (3) (2002) 299–302.
[38] K. Nithyanandam, R. Pitchumani, A. Mathur, Analysis of a latent thermocline storage system with encapsulated phase change materials for concentrating solar power, Appl. Energy 113 (2014) 1446–1460.
[39] K.E. Elfeky, X.Y. Li, N. Ahmed, L. Lu, Q. Wang, Optimization of thermal performance in thermocline tank thermal energy storage system with the multilayered PCM(s) for CSP tower plants, Appl. Energy 243 (2019) 175–190.
[40] Z. Ma, W.-W. Yang, F. Yuan, B. Jin, Y.-L. He, Investigation on the thermal performance of a high-temperature latent heat storage system, Appl. Therm. Eng. 122 (2017) 579–592.